Rankine-Hugoniot Model of Evaporation Waves in CO_2 Explosion

Hansen P.M.*, Gaathaug A.V., Bjerketvedt D., Vaagsaether K.

University of South-Eastern Norway, Department of Process, Energy, and Environmental Technology, Porsgrunn, Norway
**Corresponding author's email: perha@usn.no*

ABSTRACT

This paper presents results of small-scale experiments and calculations of rapid depressurization and evaporation of pressurized liquefied carbon dioxide (CO_2) in vertical ducts. The motivation was to quantify the damage potential of a sudden CO_2 release that originates from scenarios such as the boiling liquid expanding vapor explosion (BLEVE). The primary aim was to determine characteristic velocities and properties behind the evaporation wave as a function of the thermodynamic states ahead of the wave. Upon diaphragm rupture, a shockwave propagated outward, and a rarefaction wave propagated through the CO_2. An evaporation wave followed behind the rarefaction wave. The measured evaporation wave velocities were in the range 35–42 m/s. The expansion of the vapor headspace produced a shockwave that had a peak overpressure in the range 15–20 kPa. A Rankine-Hugoniot model that treated the phase transition as an evaporation wave calculated the fluid properties behind the wave. The model showed good qualitative agreement with the experimental results. The experimental results seemed to approach a Chapman Jouguet (CJ) solution. Typically, the calculated vapor mass fraction behind the evaporation wave was in the range from 0.21 to 0.23. The calculated vapor mass fraction was used in estimations of the energy release from a CO_2 explosion.

KEYWORDS: CO_2 explosions, BLEVE, rapid evaporation, Rankine-Hugoniot analysis.

NOMENCLATURE

h	enthalpy (J/kg)
P	pressure (Pa)
S	entropy (J/kgK)
T	temperature (K)
t	time (s)
u	velocity (m/s)
V	specific volume (m^3/kg)

Greek

γ	specific heat ratio
ρ	mass density (kg/m^3)
χ	vapor mass fraction (-)

Subscripts

0	state 0, pre-rupture state
1	state 1, ahead of the evaporation wave
2	state 2, behind the evaporation wave

INTRODUCTION

Establishing the carbon capture and storage (CCS) value chains is a part of the strategy to mitigate climate changes caused by greenhouse gas emissions. In Norway, the company Norcem is currently working on a project for capturing CO_2 from their cement production [1]. Tank explosions and pipeline ruptures in carbon dioxide (CO_2) systems are accident scenarios that happen infrequently but have the potential to cause fatalities and significant material damage. If a tank that contains a pressurized liquefied gas held at a temperature above its atmospheric pressure boiling point

Proceedings of the Ninth International Seminar on Fire and Explosion Hazards (ISFEH9), pp. 440-449
Edited by Snegirev A., Liu N.A., Tamanini F., Bradley D., Molkov V., and Chaumeix N.
Published by St. Petersburg Polytechnic University Press
ISBN: 978-5-7422-6496-5 DOI: 10.18720/spbpu/2/k19-24

ruptures, the event can be referred to as a boiling liquid expanding vapor explosion (or BLEVE). CO_2 is a non-combustible substance, and a "cold BLEVE" is a purely physical explosion. There is no heat release and no fire-ball. Nevertheless, the consequences can be severe. The hazards from a cold BLEVE include flying fragments propelled over large distances, impact damage caused by blast waves, and frost injuries caused by temperatures below 200 K. Three examples of industrial accidents in CO_2 tanks, which resulted in human fatalities and severe material damage, include the incidents in Worms, Germany [2], Repcelak, Hungary [3], and Yuhang, China [4]. Overfilling and overheating followed by excessive overpressure and brittle fracture were identified as the main reasons for these tank failures. The mitigation of future accidents requires sufficient knowledge about the physics of the rapid expansion and phase transition phenomena.

In a rapid expansion of a pressurized liquefied gas toward atmospheric pressure, the substance could cross the saturation line without undergoing a phase transition. The absence of available nucleation sites can suppress the bubble formation. The liquid then becomes superheated (or metastable) as illustrated in Fig. 1. There is a limit to the degree of superheat that a metastable liquid can obtain. The thermodynamic stability limit is given by the expression $(\partial P/\partial V)_T = 0$. The locus of states that satisfies this criterion is called the spinodal curves.

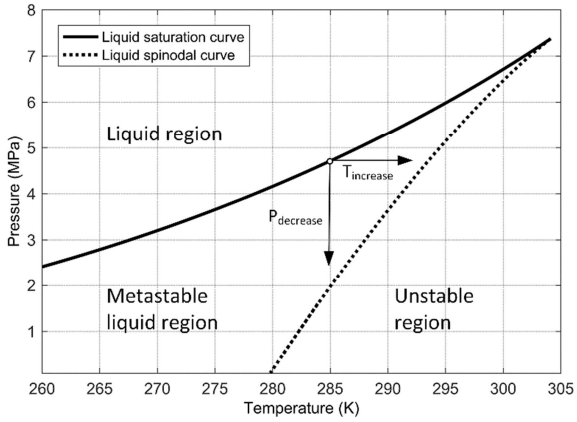

Fig. 1. p-T diagram of carbon dioxide. A saturated liquid can become superheated by decreasing the pressure or increasing the temperature. The metastable liquid region represent the possible overheat range.

In a tank rupture of a pressurized liquefied gas, the "loss of containment" results in an initial shock wave that propagates outward and a rarefaction wave that propagates through the fluid. A contact surface that initially separates the liquid and vapor phase follows behind the shock wave. At a range of superheats near the superheat limit, the phase change can take place as an evaporation wave of constant thickness that propagates behind the rarefaction fan through the metastable liquid [5]. The superheat limit represent a locus of states close to the liquid spinodal curve in Fig. 1. The propagation velocity of the evaporation wave is influenced by the thermodynamic state and the degree of superheat in the metastable liquid ahead of the wave. The energy release and damage potential can be influenced by the thermodynamic state, the vapor mass fraction, and the flow velocity behind the evaporation wave.

This study presents results from small-scale experiments and calculations on the rapid depressurization and evaporation of pressurized liquefied CO_2 in vertical ducts. A motivation was to quantify the energy release from a rapid CO_2 release. The primary aim was to determine characteristic velocities and properties behind the evaporation wave as a function of the thermodynamic states ahead of the wave. A Rankine-Hugoniot model of the evaporation wave that calculates the state behind the wave is presented. The study describes a strategy, which includes the

calculated vapor fraction, to predict the mechanical energy released in the rapid depressurization and evaporation processes. The method proposed by Prugh [6] is the starting point of the calculation method.

METHODS AND MATERIALS

The experimental setup (see Fig. 2 a) included a high-pressure vessel that was filled with pressurized liquefied CO_2 and sealed with a diaphragm at the upper end. In a previous study [7], the CO_2 was released into an atmospheric vented chamber to measure the pressure response and calculate the impulse.

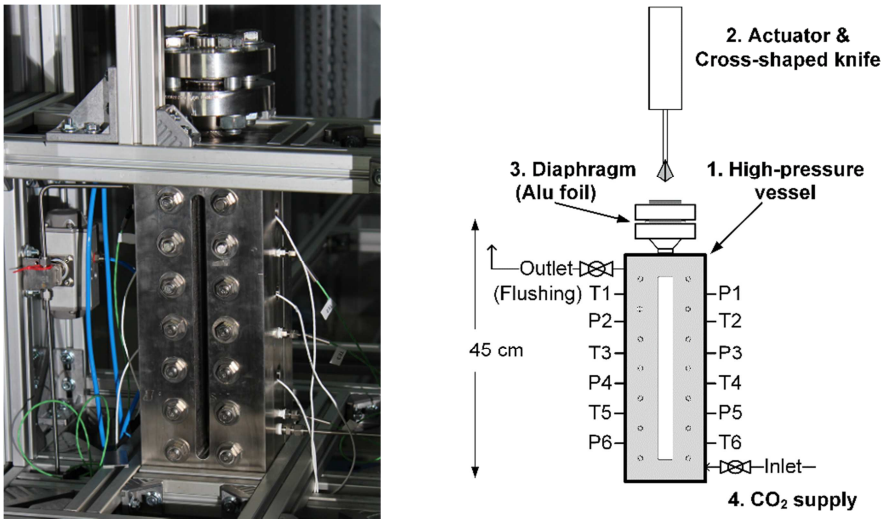

(a) (b)

Fig. 2. Experimental test setup to study rapid evaporation of CO_2 . (a) Photograph of the high-pressure vessel. (b) Schematic showing the experimental setup.

Apparatus

Figure 2 b shows a schematic diagram of the experimental setup that consisted of the following main parts: (1) a high-pressure vessel with stainless steel side-walls and borosilicate glass windows; (2) a cross-shaped knife with a pneumatic plunger actuator; (3) an aluminum foil diaphragm, and (4) a CO_2 supply-system with two industry grade cylinders. The two cylinders supplied liquid-phase and vapor-phase feed. The high-pressure reservoir was a custom-designed level gauge manufactured by PresSure Products Company and rated at 10 MPa. The vessel height from the bottom up to the diaphragm was 450 mm. The aluminum foil diaphragm was circular with a 34-mm opening diameter. The total vessel volume was 190 cm^3 with the possibility of a 130-cm^3 liquid volume.

Instrumentation

Temperature sensor ports (T1-T6) and pressure sensor ports (P1-P6) were installed on the two stainless-steel sidewalls. The vertical spacing between two adjacent sensors was 50.8 mm. The pressure transducers in the high-pressure vessel were Kulite-XTM-190-2000G piezoresistive sensors with a measuring range of 0–14 MPa, and a natural frequency of 410 kHz. The accuracy was ± 1% of the measurement range, and the thermal sensitivity shift was ± 2% per 100 K. All temperature sensors were fast-response Cromel-Alumel, K-type thermocouples with an accuracy of ± 1 K. An Ametek Jofra CTC140A unit calibrated the temperature sensors before the start of the test series.

A Photron Fastcam SA-Z camera operating at 75,000 fps, which was a part of a z-type Schlieren setup, captured the expansion and phase transition processes inside the high-pressure reservoir. Two parabolic mirrors combined with a focus lens covered a 0.127-m section of the vessel height. The presentation of these images is outside the scope of the current paper.

Test procedure and experiment control

A Quantum Composers 9500 series pulse generator initiated the experiments. A 5-volt signal triggered the knife actuator, the high-speed cameras, and the DAQ system simultaneously. The DAQ setup consisted of two HBM Quantum MX410 modules, an HBM MX440B module, and a Sigma LDS Nicolet digital oscilloscope. The cross-shaped knife punctured the diaphragm completely and with high reproducibility. The high-speed images, the temperature histories, and the pressure histories were stored and then analyzed in MATLAB. High-speed videos with sensor data included were prepared. A comparison of the image observations with the sensor measurements provided a basis for the interpretation of the experimental results. Before each test, the high-pressure reservoir was flushed three times with pressurized vapor-phase CO_2 at 1 MPa. Then, the chamber was slowly filled with either vapor-phase or liquid-phase CO_2. A ten minute idle period, between the filling stage and the test initiation provided thermal equilibrium and stable sensor measurements. The pre-rupture state was saturated CO_2 at room temperature.

Rankine-Hugoniot calculation method

The propagation of adiabatic evaporation waves was modeled by the Rankine-Hugoniot relations that treat the wave as a jump between a superheated liquid state and a 2-phase equilibrium state. This section describes the calculation method that was used. The method incorporates the ideas discussed by Simões-Moreira and Shepherd [5], Chaves [8], Hill [9], and Reinke [10]. The analysis defines three states**,** separated by a rarefaction wave (or fan), and an evaporation wave. State 0 (saturated liquid) is the initial pre-rupture state, located in front of the rarefaction wave. State 1 (superheated liquid) is the metastable liquid state, located behind the rarefaction wave but ahead of the evaporation wave. State 2 (two-phase equilibrium mixture) is located behind the evaporation wave. Figure 3 shows a control volume, which includes state 1 and 2, drawn around the evaporation wave. T is the temperature; P is the pressure; V is the specific volume; h is the enthalpy; u is the velocity; χ is the vapor mass fraction. The evaporation wave is restricted to a narrow region [5]. The enthalpy used to evaporate a fraction of the liquid originates from the rapid depressurization from the saturated liquid state to the superheated state.

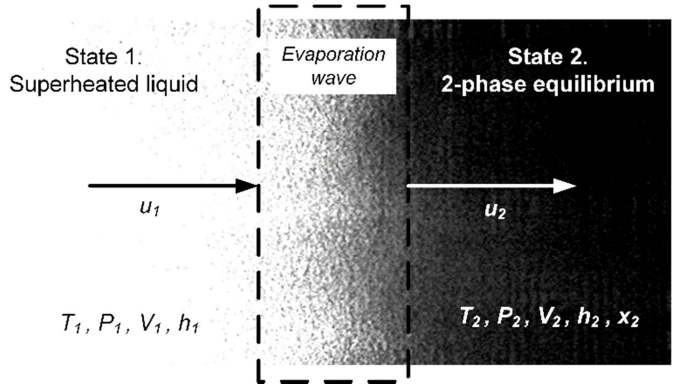

Fig. 3. Control volume that was used in the Rankine-Hugoniot analysis.

One-dimensional inviscid fluid flow is assumed with no heat transfer from the walls (adiabatic conditions). Heterogeneous nucleation on the wall surface ahead of the evaporation wave is

neglected. The method assumes both mechanical equilibrium (no slip between vapor and liquid), and phase equilibrium (saturated vapor and liquid mixture) at state 2.

The integral form of the conservation equations of mass, momentum, and energy for steady, one-dimensional flow can be formulated as:

$$\rho_1 u_1 = \rho_2 u_2 , \tag{1}$$

$$P_1 + \rho_1 u_1^2 = P_2 + \rho_2 u_2^2 , \tag{2}$$

$$h_1 + \frac{1}{2}u_1^2 = h_2 + \frac{1}{2}u_2^2 , \tag{3}$$

The velocities u_1 and u_2 are defined relative to the evaporation wave (from the wave frame of reference). The Rayleigh line (equation 4) relates the velocity u_1 to the change in pressure and specific volume across the wave. A combination of equation 1 and 2 eliminates the velocity u_2:

$$u_1 = V_1 \left(\frac{P_2 - P_1}{V_1 - V_2} \right)^{1/2} , \tag{4}$$

The Hugoniot curve (or adiabatic evaporation curve) represents a locus of possible states behind the evaporation wave. The curve combines the conservation equations 1-3 to eliminate the velocities:

$$h_2 - h_1 = \frac{1}{2}\left(P_2 - P_1\right)\left(V_2 + V_1\right) , \tag{5}$$

The enthalpy "available" for adiabatic evaporation is the enthalpy difference between the expanded and saturated liquid at pressure P_1. If u_2 is assumed to be sonic, which corresponds to a Chapman-Jouguet solution, the maximum mass flux is obtained. If phase equilibrium is assumed at state 2, the specific volume and enthalpy can be expressed by the following mixture properties:

$$V_2 = \left(1 - \chi_2\right) V_{l,2} + \chi_2 V_{v,2} , \tag{6}$$

$$h_2 = \left(1 - \chi_2\right) h_{l,2} + \chi_2 h_{v,2} , \tag{7}$$

The subscripts l, 2 and *v*,2 denotes saturated liquid and vapor at state 2. A combination of equations 5-7 results in following expression for the vapor mass fraction χ_2 at state 2:

$$\chi_2 = \frac{2\left(h_1 - h_{l,2}\right) + \left(V_1 + V_{l,2}\right)\left(P_2 - P_1\right)}{2\left(h_{v,2} - h_{l,2}\right) - \left(V_{v,2} - V_{l,2}\right)\left(P_2 - P_1\right)} , \tag{8}$$

Calculated solutions at state 2 correspond to the intersections between the Rayleigh line and the Hugoniot curve. The thermodynamic properties of CO_2 in the current study were calculated by the Span-Wagner technical equation of state [11] and a table of saturation properties from NIST [12].

RESULTS AND DISCUSSION

Figure 4 shows an x-t diagram of the depressurization process. Please note that the axes are not scaled. Upon diaphragm rupture, a shock wave propagated outward, while a rarefaction wave propagated through the CO_2 at the local speed of sound. Partial condensation of the vapor phase occurred behind the rarefaction wave. A multiphase CO_2 jet followed behind the shock wave. Wave reflections occurred at the liquid-vapor interphase and at the vessel bottom-surface. The contact surface that initially separated the liquid phase and the vapor headspace accelerated toward the high-pressure vessel exit plane. An evaporation wave followed behind the rarefaction fan. The

measured evaporation wave velocities ($W_{EW,meas}$) were in the range 35–42 m/s. Table 1 shows test parameters, experimental results and calculated properties from two test runs. A previous study [7], which was carried out on the same test setup, concluded that the rapid evaporation did not contribute to the initial shock strength in this test geometry.

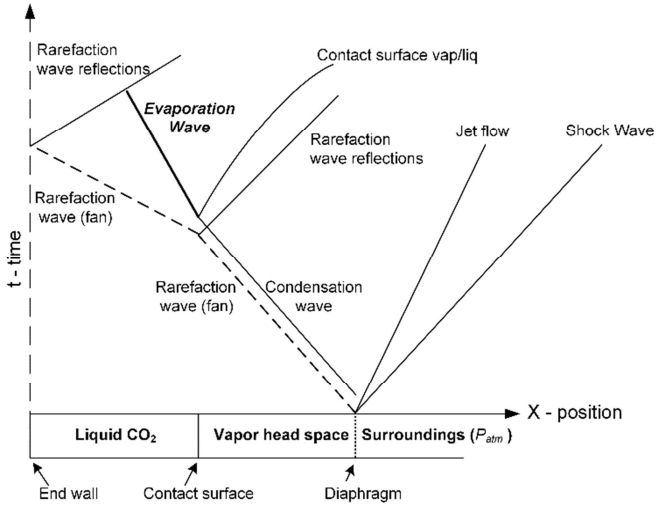

Fig. 4. x-t diagram of depressurization and phase change processes with pressurized liquified CO_2 in a duct that is initially sealed with a diaphragm.

Table 1. Initial test conditions, experimental results and calculated properties

	State	Symbol	Unit	Test 1	Test 2
Measured properties					
Pressure	0	P_0	MPa	5.8	6.3
	1	P_1	MPa	5.1	5.6
	2	P_2	MPa	3.7	4.2
Velocity	1	$W_{EW,meas}$	m/s	*35-40*	42.4
Calculated properties					
Pressure	2	P_2	MPa	3.7	4.3
Temperature	0	T_0	K	294.0	297.0
	1	T_1	K	292.5	295.5
	2	T_2	K	275.9	281.0
Density	0	ρ_0	kg/m^3	764.4	726.6
	1	ρ_1	kg/m^3	756.7	718.6
	2	ρ_2	kg/m^3	345.6	372.6
Velocities	0	u_0	m/s	3.3	3.1
	1	u_1	m/s	38.1	44.6
	2	u_2	m/s	83.5	86.1
	1	$W_{EW,calc}$	m/s	35.0	41.4
Vapor mass fraction	2	χ_2		0.22	0.23
Mass flux	2	$\dot{m}''$	kg/m^{2}s	28900	32100

These tests were designed to measure the blast from the CO_2 released into an openly vented atmospheric chamber. The measured peak overpressures were in the range 15–20 kPa. The evaporation process was too slow to contribute to the initial blast but resulted in a significantly higher impulse calculated at 100 ms [7]. Heterogeneous wall nucleation ahead of the evaporation wave seemed to limit the degree of superheat that could be achieved in this test setup.

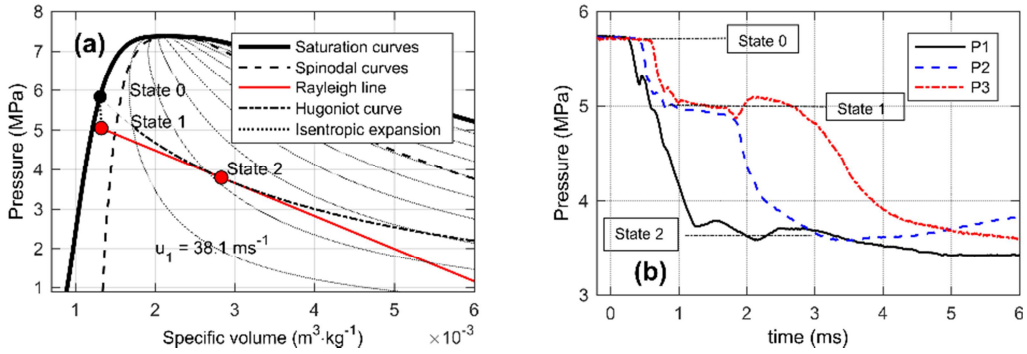

Fig. 6. Comparison of measured and calculated pressures from test 1. (a) p-V diagram with calculated state data. State 0 and 1 are specified as inputs; state 2 is calculated. (b) Pressure histories, sensors P1-P3.

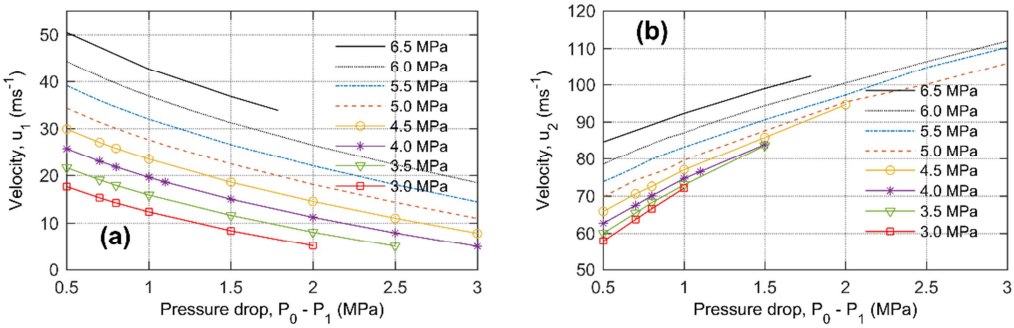

Fig. 7. Calculated CJ-solutions from the Rankine-Hugoniot analysis. Each line represents an initial pre-rupture pressure P_0. The velocities u_1 (a), and u_2 (b) were plotted as a function of the superheat pressure drop P_0 - P_1.

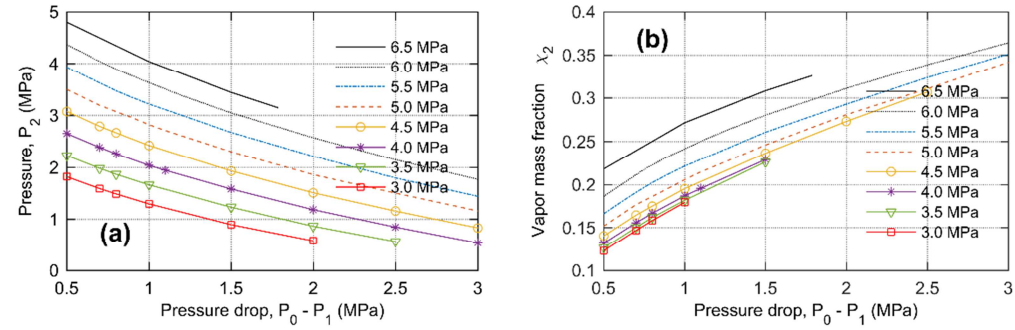

Fig. 8. Calculated CJ-solutions from the Rankine-Hugoniot analysis. Each line represents an initial pre-rupture pressure P_0 Two parameters were plotted as a function of the superheat pressure drop P_0 - P_1.
(a) The pressure behind the evaporation wave P_2. (b) the vapor mass fraction behind the evaporation wave.

Rankine-Hugoniot analysis

A Rankine-Hugoniot model that treated the evaporation wave as a jump between a metastable liquid phase and a two-phase equilibrium flow calculated the fluid properties behind the wave. Figure 6 shows plots with calculated (a) and measured (b) pressures behind the evaporation wave. The calculated pressure P_2 (state 2 in Fig. 6 a) showed good qualitative agreement with the experimental results. The experimental results seemed to approach a Chapman Jouguet (CJ) solution. At a given CJ solution, the required model inputs were the initial pre-rupture pressure and the pressure of the metastable liquid ahead of the evaporation wave. Typically, the calculated vapor mass fraction behind the evaporation wave was in the range from 0.21 to 0.23.

Figures 7 and 8 show the calculated properties ahead of and behind the evaporation wave. The plots show results from the Rankine-Hugoniot calculations that satisfy the CJ-solution for a range of pre-rupture pressures P_0 and superheat pressure drop (P_0 - P_1).

The plots in Figs. 7 and 8 provide calculation results that can be used in simple flow and state predictions. For example, if saturated liquefied CO_2 at 5.5 MPa expands to a superheated state at 4.0 MPa in a rapid isentropic process, the calculated evaporation wave velocity is approximately 27 m/s

Energy release estimate

This study suggests that the calculated vapor mass fraction χ_2 from the Rankine-Hugoniot analysis can be used to estimate the mechanical energy released in a tank explosion. If the vessel contains a pressurized liquefied gas, the fraction of liquid that rapidly evaporates could have a significant influence on the energy released at the early stage of the explosion. Several methods exist [6, 13-15] that estimates the burst energy in a BLEVE. The method proposed by Prugh [6] is the starting point of the calculation example. The current study suggests that the vapor mass fraction χ_2 calculated by the Rankine-Hugoniot relations can be incorporated in Prugh's method to provide a less conservative energy estimate. The calculated vapor mass fraction behind the evaporation wave limits the energy-release. The calculated energy- release is restricted to the vapor expansion and the phase change caused by the adiabatic evaporation wave.

If a 1-m^3 tank (see Fig. 9a) that contains 85 vol% pressurized liquefied CO_2 at 5.5 MPa in equilibrium with a CO_2 vapor headspace suddenly bursts, the mechanical energy that is released at the early stage of the explosion could be estimated by the following method. Figure 9.b shows the calculated energy-release as a function of the vapor mass fraction at state 2.

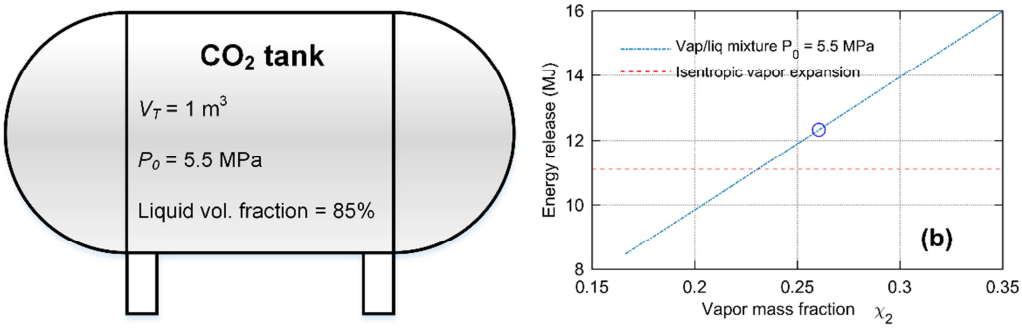

Fig. 9. Calculation example of the mechanical energy released from a CO_2 tank explosion. (a) Sketch of a CO_2 tank. (b) Energy release as a function of the vapor mass fraction χ_2.

A liquid expansion from 5.5 to 4.0 MPa gives a calculated vapor mass fraction of χ_2 = 0.26 at the CJ-solution. The specified specific heat ratio used in the calculation is γ = 1.3. The degree of

superheat in the liquid phase is considered "moderate," and heterogeneous nucleation is expected to initiate the evaporation. Thermodynamic properties of CO_2 from NIST [11] provide the density values.

Equations 9-11 show the calculation steps:

$$W_L = \rho_{0,L} \cdot V_T \cdot liq.vol.frac. = 791 \frac{\text{kg}}{\text{m}^3} \cdot 1\ \text{m}^3 \cdot 0.85 = 672\ \text{kg}\,, \tag{9}$$

$$V^* = V_T + W_L \left[\left(\frac{\chi_2}{\rho_{0,V}} \right) - \left(\frac{1}{\rho_{0,L}} \right) \right] \text{m}^3 = 1\ \text{m}^3 + 672 \left[\left(\frac{0.26}{181} \right) - \left(\frac{1}{791} \right) \right] \text{m}^3 = 1.12\ \text{m}^3\,, \tag{10}$$

$$E = \frac{PV^*}{\gamma - 1} \left[1 - \left(\frac{P_{atm}}{P_0} \right)^{(\gamma-1)/\gamma} \right] = \frac{5.5 \cdot 1.12}{1.3 - 1} \left[1 - \left(\frac{0.101}{5.5} \right)^{(1.3-1)/1.3} \right] \text{MJ} = 12.4\ \text{MJ}\,, \tag{11}$$

E is the energy released; P_0 is the initial pre-rupture pressure; P_{atm} is the atmospheric pressure; γ is the specific heat ratio; V_T is the tank volume; W_L is the mass of liquid in the tank; $\rho_{0,V}$ and $\rho_{0,L}$ are the initial densities of the vapor and liquid phase. V^* is the total volume that includes both the original vapor volume plus the volume of the vapor generated by the rapid evaporation.

The calculated mechanical energy-release was 12.4 MJ. In comparison, isentropic expansion of a pure vapor phase estimates 11.1 MJ. In this example, calculated vapor mass fractions χ_2 larger than 0.229 gives total volumes V^* larger than the volume calculated from a pure vapor expansion. The somewhat limited vapor mass fraction could explain why the rapid evaporation tests did not produce an observable shock wave.

It is important to note that the Rankine-Hugoniot calculations do not guarantee that the phase transition will occur as an evaporation wave in reality. The calculations solve the conservation equations at idealized, stationary conditions. The influence of heterogeneous nucleation is restricted to determine the superheat pressure (P_1). Homogeneous nucleation close to the superheat limit, which Reid [16, 17] proposed as a trigger for a BLEVE, is not considered here.

CONCLUSION

This paper presented results from experimental and theoretical studies of rapid expansion and phase transition of pressurized liquified carbon dioxide in a vertical duct. Results from small-scale experiments were compared with calculations from a Rankine-Hugoniot analysis. The Rankine-Hugoniot relations modeled the phase transition as an evaporation wave and calculated the fluid properties behind the wave. The model showed a good qualitative agreement with the experimental results that were sampled from three separate test setups. The measured evaporation wave velocities were 35 – 42 m/s. The experimental results seemed to approach a Chapman Jouguet solution. At a specific CJ solution, the required model inputs were the initial pre-rupture pressure and the pressure of the metastable liquid ahead of the evaporation wave. Typically, the estimated vapor mass fraction behind the evaporation wave was in the range from 0.21 to 0.23. The paper presents a strategy to predict the energy released in a tank explosion based on the calculated vapor mass fraction behind the evaporation wave.

REFERENCES

[1] Carbon capture – a part of our zero vision. https://www.norcem.no/en/carbon_capture, 2018 (accessed 10 December 2018).

[2] W.E. Clayton, M.L Griffin, Catastrophic failure of a liquid carbon dioxide storage vessel, Process Safety Progress 13 (1994) 202-209.

[3] T. Abbasi, S.A. Abbasi, The boiling liquid expanding vapour explosion (BLEVE): mechanism, consequence assessment, management, J. Hazard. Mater. 141 (2007) 489–519.

[4] Y. Zhang, J. Schork, K., Ludwig, Revisiting the conditions for a CO2 tank Explosion, Paper presented at the AIChE 2013 Spring Meeting, San Antonio, Texas, 28 April–2 May, 2013.

[5] J.R. Simões-Moreira, J.E. Shepherd, Evaporation waves in superheated dodecane, J. Fluid Mech. 382 (1999) 63-86.

[6] R.W. Prugh, Quantitative Evaluation of "Bleve" Hazards, J. Fire Prot. Eng. 3 (1991) 9-24.

[7] P.M. Hansen, A.V. Gaathaug, D. Bjerketvedt, K. Vaagsether D., Blast from pressurized carbon dioxide released into a vented atmospheric chamber, Shock Waves 28 (2018) 1053-1064.

[8] H. Chaves, Phasenübergänge und wellen bei der entspannung von fluiden hoher spezifischer wärme, PhD thesis, Georg-August-Universität, Göttingen, Germany, 1984.

[9] L.G. Hill, An experimental study of evaporation waves in a superheated liquid. Ph.D. Thesis, California Institute of Technology, Pasadena, CA, 1991.

[10] P. Reinke, Surface Boiling of Superheated Liquid, Ph.D. Thesis, ETH Zürich, 1997.

[11] R. Span, W. Wagner, A new equation of state for carbon dioxide covering the fluid region from the triple-point to 1100 K at pressures up to 800 MPa, J. Phys. Chem. Ref. Data 25 (1996) 1509–1596.

[12] E.W. Lemmon, M.O. McLinden and D.G. Friend, Thermophysical Properties of Fluid Systems in NIST Chemistry WebBook, NIST Standard Reference Database Number 69, P.J. Linstrom and W.G. Mallard (Eds.), National Institute of Standards and Technology. Gaithersburg MD, 20899, doi:10.18434/T4D303, (accessed 3 January 2018).

[13] E. Planas-Cuchi, J.M. Salla, J. Casal, Calculating overpressure from BLEVE explosion, J. Loss Prevent. Process Ind. 17 (2004) 431-436.

[14] CCPS, Guidelines for valuating the characteristics of Vapor Cloud Explosions, Flash Fires, and BLEVES. Center for Chemical Process Safety (CCPS), Published by the American Institute of Chemical Engineers, New York, 1994.

[15] C.J.H. van den Bosch, R.A.P.M. Weterings, Methods for the Calculation of Physical Effects: due to releases of hazardous materials (liquids and gases), Committee for the Prevention of Disasters, CPR 14E (TNO 'Yellow Book'), The Hague, The Netherlands, 1997.

[16] C.R. Reid, Possible mechanism for pressurized-liquid tank explosions or BLEVE's. Science 203 (4386) (1979) 1263–1265.

[17] C.R. Reid, Some theories on boiling liquid expanding vapour explosions, Fire March. (1980) 525-526.